Elastic deformation modulus for estimating convergence when tunnelling through squeezing ground

Accepted manuscript doi:
10.1680/jgeot.17.p.008

Submitted: 13 January 2017

Published online in 'accepted manuscript' format: 28 September 2017

Manuscript title: Elastic deformation modulus for estimating convergence when tunnelling through squeezing ground

Authors: Apostolos Vrakas, Weijie Dong, Georgios Anagnostou

Affiliation: ETH Zurich, Switzerland

Corresponding author: Apostolos Vrakas, Stefano-Franscini-Platz 5, 8093 Zurich, Switzerland. Tel.: +41 44 633 04 68; Fax: +41 44 633 10 97.

E-mail: apostolos.vrakas@igt.baug.ethz.ch

Accepted manuscript doi:
10.1680/jgeot.17.p.008

Abstract

Squeezing in tunnelling is commonly assessed using the linearly elastic–perfectly plastic Mohr-Coulomb (MC) model. Weak rocks and fault materials, however, exhibit confining stress-dependent and strain-hardening behaviour prior to failure, *i.e.* the higher the confining stress and the lower the shear strain the stiffer the rock behaviour. As the MC model assumes a strain- and stress-independent Young's modulus, the selection of an appropriate 'operational' value, E_{MC}, remains a major problem in tunnel studies using this model. Although E_{MC} has a significant effect on the deformation predictions (they are inversely proportional to it under small strain theory), there is no widely-accepted or well-validated approach to its selection. This paper shows, using the results of triaxial compression tests on weak rocks and fault materials from the Gotthard base tunnel and five other projects, and performing a theoretical analysis of the ground response to tunnel excavation, that E_{MC} can be determined by a simple extrapolation of standard triaxial compression test results (typically performed at lower confining pressures) to the *in situ* stress level. This is particularly useful for practical purposes as it allows standard computational methods to be used with sufficient accuracy, rendering more refined models unnecessary, at least at the preliminary design stage.

Keywords: deformation; laboratory tests; plasticity; rocks; stiffness; tunnels

Accepted manuscript doi:
10.1680/jgeot.17.p.008

INTRODUCTION

Convergence estimates for tunnels through weak rocks and fault materials prone to squeezing (*i.e.* to large deformations; see Kovári, 1998; Hoek, 2001; Barla, 2002, for relevant reviews and case studies) are widely and routinely performed assuming linearly elastic – perfectly plastic constitutive behaviour obeying the yield criterion of Mohr-Coulomb and the non-associated flow rule with a constant dilatancy angle (hereafter referred to as 'MC model'). With respect to the behaviour of the material under triaxial compression testing conditions, this model predicts that the relationships between deviatoric stress and axial strain as well as between volumetric strain and axial strain are bi-linear, while the actual stress-strain behaviour of weak rocks and fault materials (as will be shown in the following) involves irreversible strains right from the start of shearing and depends to a remarkable extent on the confining stress: the lower the shear strain and the higher the confining pressure the stiffer the material behaviour. The latter implies that even in the ideal case of a bi-linear stress-strain relationship (*i.e.* in the absence of strain-hardening), the elastic modulus would depend on the confining stress.

In deep tunnels, there is a significant variation in the stresses and strains in the surrounding ground after excavation. Specifically, radial stress decreases from the *in situ* stress (prevailing far from the tunnel) to a relatively low support pressure at the tunnel wall, while deformations increase around the opening. It becomes evident that the closer a point is to the tunnel, the lower the stiffness of the ground. As will be shown later, the stiffness-variation reaches up to one order of magnitude. The selection of an adequate 'operational' elastic modulus (E_{MC}) for the MC model is therefore challenging and, at the same time, of great importance from an engineering viewpoint, as the MC model predicts tunnel convergences that are inversely proportional to E_{MC} under small strain theory (Anagnostou & Kovári, 1993). However, there

Accepted manuscript doi:
10.1680/jgeot.17.p.008

is no widely-accepted or well-validated approach for selecting an adequate value based upon the results of triaxial tests.

The existing studies related to confining stress-dependent rock stiffness either determine stiffness stress-dependency based upon laboratory or *in situ* tests (considering certain elastic moduli) disregarding the tunnel boundary value problem (Kulhawy, 1975a; Verman *et al.*, 1997; Asef & Reddish, 2002) or apply a variable elastic modulus in the elastic or elasto-plastic analysis of the boundary value problem (Kulhawy, 1975b; Santarelli *et al.*, 1986; Brown *et al.*, 1989; Duncan Fama & Brown, 1989; Ewy & Cook, 1990; Nawrocki & Dusseault, 1995). There is therefore still a missing link between the experimentally observed behaviour and the analysis of even the classic ground response tunnel problem. (Note that in the case of applying a variable elastic modulus, it is not clear which of the possible moduli that can be defined on a non-linear stress-strain curve should be considered, as will be explained in detail in the following).

More refined constitutive models are better at mapping the rock behaviour observed in experiments and they thus render the estimation of an operational modulus unnecessary. They do, however, require numerical calculations with special software and, in many cases, a very large collection of parameters, which explains the popularity of the MC model in tunnel design. This paper draws on experimental results and theoretical analysis to investigate whether it is possible to determine an operational modulus for the MC model, such that the resulting predictions are similar to those from advanced models that are capable of reproducing the experimentally observed behaviour.

The paper firstly presents and discusses a wide collection of data on experimental results from triaxial compression tests performed at the Rock Mechanics Laboratory of ETH Zurich on kakirites from the Gotthard base tunnel as well as on weak rocks and fault materials from

five other project sites. The experimental results substantiate the statements made above concerning actual behaviour, showing among other things that both the secant and the unloading-reloading stiffness moduli follow a power law. Subsequently, it is shown that a simplified version of the well-known Hardening Soil model (Schanz *et al.*, 1999) is capable of reproducing the basic aspects of the experimentally observed behaviour much better than the MC model.

As this constitutive model (hereafter referred to as 'SHS model') is better than the MC model at describing the behaviour of various weak rocks and fault materials in response to triaxial compression, the following two plausible assumptions can be made: (a) that it will be better at predicting the ground response also for other stress paths, including those followed by the ground around tunnels, thus providing a benchmark for the adequacy of the MC model; (b) that the laboratory rock specimen parameters are representative of the rock mass behaviour, which is a reasonable assumption as these rocks are intensively sheared up to the specimen scale (the effect of discontinuities in the scale of the opening is of subordinate importance). To this end, a computational method is developed for the axisymmetric ground response problem according to the SHS model and, finally, it is shown through a wide parametric study that the MC model can be adequately calibrated for convergence assessments in tunnelling considering the information from triaxial compression tests: by taking the elastic modulus equal to the E_{50} secant modulus that corresponds to the *in situ* stress level.

ROCK BEHAVIOUR IN DRAINED TRIAXIAL COMPRESSION

Kakiritic rocks from the Gotthard base tunnel

A long experimental study was carried out at the Rock Mechanics Laboratory of ETH Zurich during the planning and construction of the Gotthard base tunnel (Switzerland), whose excavation was successfully completed recently. With regard to the weak kakiritic rocks that

Accepted manuscript doi:
10.1680/jgeot.17.p.008

were encountered along the Sedrun section, 90 consolidated drained triaxial compression (CD-TC) tests were performed (55 of them during the first experimental campaign (Vogelhuber, 2007) and 35 of them during the second experimental campaign (Anagnostou *et al.*, 2008)). Table 1 summarizes the corresponding test results in terms of the strength and dilatancy parameters of the MC model as well as of the deformation moduli during primary loading (represented by the modulus E_{50}) and during unloading-reloading (represented by the modulus E_{ur}; in the cases that two unloading-reloading cycles were performed, E_{ur} corresponds to the average modulus of these two cycles). The low strength and high deformability of the material in combination with the high overburden (up to 900 m) led to the expectation of squeezing conditions and thus to a special design (for details see Kovári *et al.*, 2000).

Two typical kakiritic samples from the first campaign are considered first in order to show the mechanical behaviour of the material (No. 50 and No. 51 in Table 1). The samples stem from a core sample cut into two pieces and subjected to single-stage triaxial compression tests under confining pressures of 6 and 1 MPa, respectively. The strength parameters were thus determined for both samples. Figure 1 (black curves) shows the stress–strain relationship and the volumetric strain evolution for each confining pressure (the upper diagrams correspond to σ_3 = 6 MPa and the lower diagrams to σ_3 = 1 MPa). The deviatoric stress and volumetric strain are defined as follows:

$$q = \sigma_1 - \sigma_3, \quad \varepsilon_{vol} = \varepsilon_1 + 2\varepsilon_3, \tag{1}$$

where σ_1, ε_1 and σ_3, ε_3 denote the major (axial) and minor (radial) principal stresses and strains, respectively, with compressive stresses and strains taken as positive.

Additionally, two samples are considered from the second campaign (No. 63 and No. 64 in Table 1). The samples were subjected to multi-stage triaxial compression tests under

confining pressures of 2, 5 and 9 MPa. The strength parameters were thus determined separately for each sample. Figures 2 and 3 (black curves) show the test results for each sample at the first loading stage.

According to Figures 1 to 3, the mechanical behaviour of kakirites is characterized by: (a) highly non-linear stress-strain relationships with irreversible strains right from the start of loading; (b) stiffer behaviour in response to unloading-reloading than to loading; (c) confining stress–dependent stress-strain behaviour in both loading and unloading-reloading; (d) no decrease in strength (or a minor decrease in a few samples not shown here) up to axial strains of 5 to 10% even at low confining stresses, *i.e.* strain-hardening (or ductile) behaviour, and; (e) volumetric strain rate initially positive (volume decrease), changing later to negative (dilatancy occurs practically at a constant rate after some shearing, which justifies the computational assumption of a constant non-zero dilation angle at failure).

As a measure of the observed stiffness, the following common moduli will be considered (Fig. 4): the unloading-reloading modulus, denoted by E_{ur}, and the secant modulus in primary loading at a deviatoric stress equal to half the failure stress, denoted by E_{50}. Table 1 summarizes the values of these moduli for the kakiritic samples and Figure 5 (circular marks) plots them as a function of the transformed confining stress. Specifically, normal stresses are transformed by the theoretical biaxial tensile strength (Caquot, 1934):

$$\bar{\sigma} = \sigma + c_f \big/ \tan\varphi_f \,, \tag{2}$$

where c_f and φ_f denote the cohesion and the friction angle at failure, respectively (Table 1). Figure 5 shows that, (a), the higher the confining pressure the stiffer the material behaviour and, (b), the behaviour in response to unloading-reloading is stiffer than the behaviour in response to primary loading (at the same confining pressure). Moreover, it indicates that both

moduli obey approximately the following power law (*cf.* Janbu, 1963, 1985; Duncan & Chang, 1970):

$$E = E_{ref}\left(\frac{\bar{\sigma}_3}{\bar{\sigma}_{3,ref}}\right)^n, \tag{3}$$

where the reference modulus E_{ref} corresponds to a reference minor principal stress of $\sigma_{3,ref}$ and n denotes the slope of the line in a bi-logarithmic representation. It should be noted that other power laws have also been proposed for describing the dependency of rock stiffness on stress (*e.g.* Kulhawy, 1975a; Santarelli *et al.*, 1986; Brown *et al.*, 1989; Ewy & Cook, 1990; Verman *et al.*, 1997; Asef & Reddish, 2002), but Eq. (3) has proven to be sufficient for the materials examined here.

As mentioned earlier and shown in Table 1, both single-stage and multi-stage tests were performed. Although a multi-stage test is obviously advantageous for determining the strength parameters as well as the stress-dependency of the E_{ur} modulus (as a single specimen is required; *cf.*, *e.g.*, Lumb, 1964), it provides only a single value for the E_{50} modulus – the value from the first loading stage. The corresponding values from the later loading stages are quite high and cannot be considered representative. The reason for this is the deformation history of the material. Specifically, the samples have not been pre-sheared before first loading and thus no deviatoric hardening has occurred. At the later loading stages, however, the samples have become stiffer due to shearing during the first stage and the corresponding E_{50} moduli increase remarkably (*cf.* Saeedy & Mollah, 1988). Therefore, only the E_{50} moduli determined from the first loading stage are considered here for evaluating material behaviour and plotted in Figure 5. By contrast, all loading stages are considered for the unloading-reloading modulus E_{ur}, because the latter is shown to be unaffected by the pre-shearing. From a computational viewpoint, this observation supports the hypothesis of an elastic domain

Accepted manuscript doi:
10.1680/jgeot.17.p.008

inside the yield surface, *i.e.* the material behaviour in response to unloading-reloading after elasto-plastic shearing can be assumed to be elastic (this assumption is made in the SHS model formulated below).

Finally, it should be pointed out that the ultimate dilation angle, indicated by the slope of the volumetric strain over axial strain line after a sufficient amount of shearing, also depends on the confining stress (as the stiffness moduli). However, the variation is not significant (see Figure 1 and Table 1) and the dilation angle can thus be taken as a constant.

Other rock types from various project sites

This section outlines the behaviour of various weak rocks and fault materials under triaxial compression testing conditions and compares it with the behaviour of the kakirites from the Gotthard base tunnel. The tested samples come from five projects in which squeezing conditions were or are expected; detailed experiments were thus performed at the Rock Mechanics Laboratory of ETH Zurich in order to investigate the geomechanical behaviour of the corresponding materials (see Table 2):

(1) the Ceneri base tunnel (the second largest tunnel of the Gotthard axis in Switzerland), whose excavation was recently completed without finally encountering significant squeezing problems (the laboratory investigations are described in Anagnostou & Pimentel, 2004 and Anagnostou *et al.*, 2011);

(2) the Visp tunnel in Switzerland (under construction; the laboratory investigations are described in Anagnostou & Pimentel, 2005 and Pimentel & Anagnostou, 2014);

(3) the planned Seich-Sou tunnel in Greece (the laboratory investigations are described in Anagnostou *et al.*, 2010);

(4) the planned Semmering base tunnel in Austria (the laboratory investigations are described in Pimentel *et al.*, 2014) and;

(5) the planned second tube of the Karawanks tunnel connecting Slovenia and Austria (significant squeezing conditions were encountered during construction of the first tube, Schubert & Marinko, 1989; the laboratory investigations are described in Pimentel & Anagnostou, 2017).

Figures 6 to 10 show typical stress-strain relations (left-hand side diagrams) and volumetric strain evolutions (right-hand side diagrams) for each material. The mechanical behaviour is qualitatively similar to that of the Gotthard kakirites. Figure 5 (triangular marks) includes the deformation moduli E_{50} and E_{ur} for these materials.

It can be concluded that, (a), both stiffness moduli follow approximately a linear relationship in the bi-logarithmic plane (according to Eq. 3) and, (b), the slope n can be taken equal in primary loading and in unloading-reloading. Considering that the unloading-reloading phase is less sensitive to disturbance and that there are more E_{ur} values (specifically, the number of E_{50} values equals the number of specimens, while the number of E_{ur} values is much higher), it is more appropriate to calculate the constant n based upon the E_{ur} modulus. For the investigated materials it is equal to 0.6 – 1.0 (Table 2).

CONSTITUTIVE MODELLING OF WEAK ROCKS AND FAULT MATERIALS

Description of the MC model

The MC model assumes linearly elastic–perfectly plastic behaviour. Elastic behaviour is governed by Hooke's law and requires two material constants: the Young's modulus E and the Poisson's ratio v. The plastic behaviour obeys the yield function

$$Y = \bar{\sigma}_1 - \frac{1+\sin\varphi_f}{1-\sin\varphi_f}\bar{\sigma}_3 = 0 \tag{4}$$

and the plastic flow rule

$$\frac{\mathrm{d}\varepsilon_3^{pl}}{\mathrm{d}\varepsilon_1^{pl}} = -\frac{1}{\zeta}\kappa = -\frac{1}{\zeta}\frac{1+\sin\psi_f}{1-\sin\psi_f}, \tag{5}$$

where ψ_f denotes the dilation angle at failure. The variable ζ is introduced in order to distinguish between triaxial compression ($\zeta = 2$) and plane strain ($\zeta = 1$) conditions. The triaxial formulation is considered in the evaluation of the testing results and is based upon Koiter's (1953) flow rule, while the plane strain formulation applies to the boundary value problem examined later, disregarding the possibility of plastic flow in the out-of-plane direction.

Calibration of the MC model

The MC model has five parameters in total (E, ν, c_f, φ_f and ψ_f). As explained earlier, the selection of a Young's modulus presents difficulties since the actual stress-strain behaviour is non-linear and dependent on the confining stress. The Poisson's ratio is typically between 0.2 and 0.35. The shear strength parameters c_f and φ_f can be determined from the slope (= $\left(1+\sin\varphi_f\right)/\left(1-\sin\varphi_f\right)$) and the intersection (the uniaxial compressive strength $\sigma_D = 2c_f\cos\varphi_f/\left(1-\sin\varphi_f\right)$) of the corresponding stress states at failure (after Eq. 4; in the case of a multi-stage test a single sample is sufficient, while at least two samples are required for single-stage tests). Finally, the dilation angle can be determined from the slope of the volumetric to the axial strain at failure, which equals κ–1 (after Eq. 5). As mentioned earlier, the dependency of the dilation angle to the confining stress is not significant and can thus be taken as a constant.

Predictions of the MC model

Figure 1 includes the MC bi-linear predictions (red curves) for the kakiritic samples. The Young's modulus is taken equal to the E_{50} modulus at σ_3 = 6 MPa. Although the MC model

produces a rough approximation of the actual rock behaviour in response to primary loading at the confining pressure of 6 MPa (Fig. 1a), it leads to totally erroneous results at the confining pressure of 1 MPa (Fig. 1b), overestimating deviatoric stresses and dilatant volumetric strains. (Note that the higher the Young's modulus, the lower the axial strain at the onset of yielding and, consequently, the lower the maximum elastic/contractant volumetric strain and the higher the plastic/dilatant volumetric strain.) At the same time, the unloading-reloading stiffness is underestimated. However, taking the Young's modulus equal to the E_{50} modulus at σ_3 = 1 MPa would lead to an underestimation of stresses and dilatant volumetric strains at the confining pressure of 6 MPa, while taking the Young's modulus equal to the E_{ur} modulus at σ_3 = 6 MPa, would obviously lead to a much greater overestimate of stresses and volumetric strains in response to primary loading at both confining pressures. Figures 2, 3 and 6–9 include the MC predictions (red curves) for the rest of the samples tested. The E_{50} modulus at the reference confining pressure of each sample is considered again. The results verify that the MC model reproduces the actual material behaviour poorly, even at the confining pressure under which the E_{50} modulus is measured.

Basic considerations on the SHS model

The constitutive model used to map the experimental results is based on the Hardening Soil model of Schanz *et al.* (1999) and Benz *et al.* (2008). It is referred here to as simplified Hardening Soil model, as it constitutes a simplified version of the original model (in that it neglects volumetric hardening), and it will be described below.

The SHS model adopts the basic idea that stress-strain behaviour during primary loading in triaxial compression tests fulfils Duncan & Chang's (1970) hyperbolic relationship (which is based upon Kondner's (1963) relationship), according to which the axial strain is related to the deviatoric stress as follows (Fig. 4):

$$\varepsilon_1 = \frac{q}{2E_{50}} \frac{1}{1 - q/q_a}, \quad q < q_f \,. \tag{6}$$

The deviatoric stress at failure q_f satisfies the Coulomb criterion (Eq. 4) and is taken equal to a fraction of the asymptotic stress q_a:

$$q_f = \frac{2\sin\varphi_f}{1-\sin\varphi_f}\bar{\sigma}_3 = R_f q_a \,, \tag{7}$$

where R_f is a constant (commonly close to unity). For shear stresses greater than q_f the behaviour is assumed to be perfectly plastic.

Although E_{50} equals the secant stiffness in primary loading at half the asymptotic stress according to Eq. (6), the deviatoric stress at failure is considered instead when calibrating triaxial compression test results (see Fig. 4). The difference is negligible provided that R_f is close to unity.

In order to formulate an elasto-plastic constitutive model exhibiting the behaviour expressed by Eq. (6), the additive strain decomposition into elastic and plastic parts has to be considered first: $\varepsilon_1 = \varepsilon_1^{el} + \varepsilon_1^{pl}$. Under conditions of triaxial compression, Hooke's law implies that $\varepsilon_1^{el} = q/E_{ur}$. Defining the accumulated plastic deviatoric strain as the hardening parameter, that is,

$$\gamma^{pl} = \varepsilon_1^{pl} - \varepsilon_3^{pl} \,, \tag{8}$$

and assuming that plastic volumetric strains are negligible, which leads to

$$\gamma^{pl} = \frac{3}{2}\varepsilon_1^{pl} - \frac{1}{2}\varepsilon_{vol}^{pl} \cong \frac{3}{2}\varepsilon_1^{pl} \,, \tag{9}$$

Eq. (6) then becomes

$$\frac{3}{4}\frac{q}{E_{50}}\frac{1}{1-q/q_a} - \frac{3}{2}\frac{q}{E_{ur}} - \gamma^{pl} = 0, \quad q < q_f \,. \tag{10}$$

Both stiffness moduli are considered to be stress-dependent according to Eq. (3) (with $E = E_{50}$ and $E = E_{ur}$, respectively). It can easily be shown that Eq. (10) leads to practically the same hyperbolic stress-strain curve irrespective of the amount of dilatancy. In other words, the assumption of zero dilatancy made in Eq. (9) is not essential with respect to the validity of Eq. (6) for realistic ground mechanical properties. It has finally to be noted that Eq. (10) requires that $E_{ur} > 2E_{50}$. This was shown always to be the case for the materials examined here (see for example Table 1).

Yield function and plastic flow rule of the SHS model

The SHS model assumes that Eq. (10) can be generalized in the three-dimensional principal stress space. The yield function can then be written as follows (similarly to Eq. 4):

$$Y = \bar{\sigma}_1 - \frac{1+\sin\varphi_m}{1-\sin\varphi_m}\bar{\sigma}_3 = 0, \tag{11}$$

where φ_m denotes the secant mobilized friction angle in the transformed stress plane (transformation of Eq. 2 is still used here), which satisfies the hardening rule of Eq. (10) with

$$q = \frac{2\sin\varphi_m}{1-\sin\varphi_m}\bar{\sigma}_3 \tag{12}$$

(by additionally setting q_a after Eq. 7, Eq. 10 is expressed in terms of σ_3, φ_m and γ^{pl}; therefore, for a certain value of the hardening parameter γ^{pl}, Eq. 11 resembles a non-linear – or linear for $n = 1$ – yield curve in the σ_3–σ_1 plane).

Moreover, a linear plastic flow rule is considered (similarly to Eq. 5):

$$\frac{\mathrm{d}\varepsilon_3^{pl}}{\mathrm{d}\varepsilon_1^{pl}} = -\frac{1}{\zeta}\kappa_m = -\frac{1}{\zeta}\frac{1+\sin\psi_m}{1-\sin\psi_m}, \tag{13}$$

where ψ_m denotes the mobilized dilation angle, which is taken according to Rowe's (1962) relation:

$$\sin\psi_m = \frac{\sin\varphi_m - \sin\varphi_c}{1 - \sin\varphi_m \sin\varphi_c}. \quad (14)$$

It is repeated here that the variable ζ was introduced in order to distinguish between triaxial compression ($\zeta = 2$) and plane strain ($\zeta = 1$) flow conditions. The critical mobilized friction angle φ_c is such that the material will experience a positive volumetric strain rate (*i.e.* its current volume will decrease) as long as $\varphi_m < \varphi_c$ and dilate as long as $\varphi_m > \varphi_c$. It can be defined in terms of the ultimate values of the friction and dilatancy angles as follows (see Schanz & Vermeer, 1996):

$$\sin\varphi_c = \frac{\sin\varphi_f - \sin\psi_f}{1 - \sin\varphi_f \sin\psi_f}. \quad (15)$$

It is noted that φ_c could be used as a direct input parameter (instead of the dilation angle at failure), but, as explained earlier, the estimation of ψ_f is straightforward. Eq. (15) was shown to map the experimental results for the Gotthard kakirites reasonably well (see following sections).

Finally, it should be noted that the elastic part of the SHS model, which is based on Hooke's law with a variable Young's modulus E_{ur} according to Eq. (3), is not conservative (*cf.*, *e.g.*, Zytynski *et al.*, 1978; Lade & Nelson, 1987), but this can be accepted for monotonic loading conditions. Furthermore, the yield and failure surfaces have a hexagonal shape in the deviatoric plane disregarding any potential effect of the intermediate principal stress.

Calibration of the SHS model

The SHS model incorporates eight parameters, which have clear physical meanings and can be determined from conventional triaxial compression tests: four of them are the same as in the MC model (ν, c_f, φ_f, ψ_f) and another four are used to determine the stress-dependent stiffness ($\sigma_{3,ref}$, $E_{50,ref}$, $E_{ur,ref}$, n; Eq. 3). The constant R_f is always set close to unity (0.80 –

Accepted manuscript doi:
10.1680/jgeot.17.p.008

0.95) and can be either assumed *a priori* or selected to provide a better fit to the experimental results.

Predictions of the SHS model

Figure 1 includes the SHS model predictions (blue curves) for the two kakiritic samples. The model maps the observed mechanical behaviour well. The reference confining stress $\sigma_{3,ref}$ is taken equal to 6 MPa and the moduli $E_{ur,ref}$ and $E_{50,ref}$ are thus directly determined from the test results of Figure 1a. The exponent n was determined considering the unloading-reloading modulus at all loading stages of all the kakiritic samples (see Table 2), while the constant R_f was set equal to 0.85 in order to have a better fit. Finally, the dilation angle was set equal to 4.7°. The SHS model also reproduces the experimental results under the confining stress of 1 MPa well, as it explicitly accounts for the stiffness stress-dependency. It can, of course, also map the specimen's stiffness in response to unloading-reloading.

Figures 2, 3 and 6–10 include the SHS predictions (blue curves) for the remaining samples. They verify that the SHS model is adequate for describing the behaviour of various weak rocks and fault materials in response to triaxial compression. The assumption can thus be made that they are also adequate for describing the ground response to other loading conditions and in turn to tunnel excavation.

GROUND RESPONSE ANALYSIS WITH THE SHS MODEL

Problem description

The classic problem of a deep circular tunnel of radius a_0 under plane strain, rotationally symmetric conditions is studied here. The initial stress field is assumed to be uniform and isotropic of magnitude σ_0 and the support pressure σ_a is gradually reduced from σ_0 to zero. Consequently, the major and minor directions represent the tangential and radial directions, respectively.

Accepted manuscript doi:
10.1680/jgeot.17.p.008

For the response of a MC ground to tunnel excavation, the standard and widely-used small strain closed-form solution is used (*e.g.* Panet, 1995), in combination with the equation given by Vrakas & Anagnostou (2015) to account for large strain effects (this correction leads to virtually identical results with the exact large strain solution; Vrakas & Anagnostou, 2014). For the SHS model, a simple computational method is used (presented in the Appendix together with its validation). The method was inspired by that of Lee & Pietruszczak (2008) for a material exhibiting strain-softening and is based on the existence of a unique stress-strain path followed by every material point around the tunnel. Although the method presented is formulated in the framework of small strain theory, application of the equation given by Vrakas & Anagnostou (2015) leads to highly accurate large strain analysis results (as shown in the Appendix by means of comparisons with an exact closed-form SHS solution, which is derived under certain simplifying assumptions).

Any potential effect of the intermediate principal stress is disregarded, *i.e.* the out-of-plane stress is assumed to remain the intermediate principal stress throughout unloading. Although an extension of the computational method to account for the corner flow that may take place at lower support pressures is trivial, it is known that the predicted convergences in the MC problem remain practically unaltered (Reed, 1988; Cantieni & Anagnostou, 2009) and therefore there is no essential reason to overload the analytical part of the study by considering out-of-plane plastic flow.

Outline of the ground response

Figure 11 presents the normalized stress (a) and shear strain (b) distributions around an unsupported tunnel according to the SHS (solid curves) and the MC (dashed curves) models, now considering the complete parameter set of Figure 1 (without the assumptions made for the validation of the computational method). Despite the fact that the SHS model reproduces

Accepted manuscript doi:
10.1680/jgeot.17.p.008

all the basic aspects of the mechanical behaviour of kakirites that the MC model does not (stiffness stress-dependency, strain-hardening, variable dilatancy), Figure 11b shows that significant shearing occurs mainly within a zone of similar extent. However, as there is no fully elastic ring around the tunnel according to the SHS model (plastic deformations develop right from the start of shearing, that is, the plastic ring around the tunnel extends up to an infinite distance from its centre), the tangential stress presents a smooth variation around the tunnel, in contrast to the MC model which predicts a peak.

Figure 12 shows the corresponding GRCs. As explained earlier, the MC model can lead to several curves (dashed curves), depending on the elastic modulus chosen, while the SHS model predicts a unique curve (solid curve). More specifically, considering that the power law of Eq. (3) describes the material stiffness over the entire stress range around the tunnel sufficiently well (Fig. 5), *i.e.* from zero to 20 MPa, both the secant modulus E_{50} and the unloading-reloading modulus E_{ur} can be used as reference values. An evaluation of Eq. (3) for both moduli at three stress levels that are realistic (or possible) at first sight (σ_3 = 1 MPa, that is close to the tunnel wall; 10 MPa, that is around the plastic radius; and 20 MPa, that is in the far field) leads to six parameter sets and thus six GRCs (dashed curves).

DEFORMATION MODULUS FOR SQUEEZING ASSESSMENTS IN TUNNELLING

Basic considerations

Figure 12 shows that the range of MC tunnel convergences obtained is very large, since the elastic modulus varies to remarkable extent and the calculated convergences increase strongly with decreasing modulus (inversely proportional to it when neglecting geometric non-linearity; Anagnostou & Kovári, 1993). Nevertheless, the MC predictions (dashed curves) are very close to the SHS prediction (solid curve) for certain values of the Young's modulus (E_{50} at σ_3 = 20 MPa and E_{ur} at σ_3 = 1 MPa), thus indicating that it may be possible to determine an

appropriate 'operational' modulus. In order to establish a general method for estimating this 'operational' modulus, however, we have first to verify the sensitivity of the SHS predictions for the two moduli considered.

To this end, Figure 13 plots the GRCs according to the SHS model, (a), for a fixed E_{50} modulus and three different values for the E_{ur} modulus and, (b), for a fixed E_{ur} modulus and three different values for the E_{50} modulus (E_{ur} = 2.5/5/10 E_{50} in both cases). Clearly, the sensitivity of the results to the secant modulus is much higher and the operational deformation modulus for the MC model should therefore be defined in terms of E_{50} and not E_{ur}. Of course, this conclusion does not invalidate the usefulness of measuring the unloading-reloading modulus in triaxial tests, since (as explained previously) this is the best way to quantify stiffness stress-dependency, expressed here by the exponent n. It does show, however, that from a computational viewpoint the value of the unloading-reloading modulus is of secondary importance for predicting tunnel convergences. What affects the predicted convergences to a remarkable extent is the stiffness in response to primary loading, expressed here by the E_{50} modulus.

With regard to the confining stress at which the secant modulus has to be taken, the following heuristic reasoning has proven valuable: As shown by Kovári (1985, 1998) based upon small strain kinematic considerations and neglecting the elastic deformations within the plastic zone, tunnel convergence u_a is related to the radial displacement u_ρ at the elasto-plastic interface by the simple equation $u_a = u_\rho \left(\rho/a_0\right)^\kappa$, where ρ denotes the radius of the plastic zone ($\rho/a_0 = \left(\bar{\sigma}_\rho/\bar{\sigma}_a\right)^{\left(1-\sin\varphi_f\right)/2\sin\varphi_f}$) and u_ρ is obtained applying Kirsch's equations to the outer elastic zone ($u_\rho = \rho\left(\sigma_0 - \sigma_\rho\right)\left(1+\nu\right)/E$, where σ_ρ is the radial stress at $r = \rho$, $\bar{\sigma}_\rho = 2\bar{\sigma}_0/\left(m+1\right)$). As E appears only in the equation for u_ρ (ρ and σ_ρ do not depend on E),

Accepted manuscript doi:
10.1680/jgeot.17.p.008

which applies to the outer elastic domain, where the mean stress is constant and equal to the *in situ* stress σ_0, it seems promising to take E equal to the secant modulus that corresponds to the *in situ* stress σ_0:

$$E_{MC} = E_{50,ref}\left(\frac{\bar{\sigma}_0}{\bar{\sigma}_{3,ref}}\right)^n. \quad (16)$$

Validation of the proposed equation

The calibration of the MC model with the aid of Eq. (16) will be examined first for the Gotthard kakirites, considering the unsupported wall displacement of a deep axisymmetric tunnel, which constitutes a characteristic measure commonly used to indicate potential squeezing problems in tunnelling (*e.g.* Barla, 2002). The computations were performed for all parameter sets of Table 1 (the dilation angle was taken equal to 5° for the samples without sufficient data).

Figure 14 plots the convergences obtained from the MC model using the elastic modulus after Eq. (16) (vertical axis) with those from the SHS model (horizontal axis). Every point corresponds to another material parameter set of Table 1. The results lie practically on the angle bisector, indicating that Eq. (16) is adequate.

Motivated by this outcome, an extended parametric study is performed next to generally validate Eq. (16) for a very wide range of parameters (material constants, initial stresses and support pressures; see Table 3), leading to 1620 combinations in total. Figure 15 shows the predicted tunnel wall displacements according to both models. The results are again very close to the angle bisector.

Consequently, the MC model can be calibrated for weak materials (not actually exhibiting the behaviour predicted by the MC model) by selecting the appropriate operational deformation modulus E_{MC}. This operational modulus is defined as the modulus that leads to MC tunnel

Accepted manuscript doi:
10.1680/jgeot.17.p.008

convergences similar to those obtained from the SHS model and given by Eq. (16), according to which the measured secant modulus in a triaxial compression test, $E_{50,ref}$, has to be extrapolated to the *in situ* stress level. The exponent n that defines the stress-dependency is considered as a material constant. For the materials tested, n varies from 0.6 to 1.0 (Table 2), indicating a remarkable stress-dependency.

CONCLUSIONS

This paper showed that the widely-used MC model can be used for reliable ground response assessments in tunnelling in spite of its apparent oversimplifications, provided that the Young's modulus is determined appropriately. The paper was divided in four parts: (a) an experimental part, which presented triaxial compression test results on weak rocks and fault materials from the Gotthard base tunnel and from four other project sites; (b) a theoretical part, which showed the limitations of the widely-used MC model and outlined a simplified Hardening Soil model that can reproduce the observed mechanical behaviour considerably better; (c) an analytical part, which investigated the corresponding ground response to tunnel excavation by means of a computational method developed for materials satisfying the SHS model; and (d) an application part, which showed that the MC model can be calibrated to predict tunnel convergences correctly for materials not actually exhibiting MC behaviour by selecting an appropriate operational deformation modulus, given by a simple formula that is based upon triaxial compression test results.

The approach presented allows conventional computational methods (for axisymmetric circular tunnels) based upon the MC model to be used for squeezing assessments in tunnelling, rendering the performance of more demanding analyses based on more sophisticated constitutive models unnecessary, at least for preliminary studies. In problems where the ground response (or convergence-confinement; *e.g.* Panet, 1995) design concept

does not apply (Cantieni & Anagnostou, 2009) as well as in more complicated tunnel analyses, a Hardening Soil-type model should be used.

ACKNOWLEDGEMENTS

The paper evolved within the framework of the research project 'On the role of constitutive behaviour in the response of squeezing ground to tunnelling', which is being carried out at the ETH Zurich with the financing of the Swiss National Science Foundation under Project No. 137888.

Appendix. GROUND RESPONSE WITH THE SHS MODEL

This Appendix presents a semi-analytical (explicit) computational method for the calculation of the ground response to tunnel excavation under plane strain rotationally symmetric conditions, considering that the ground satisfies the SHS constitutive model.

Computational method

A hollow cylinder of inner radius a_0 and (initially unknown, but >> a_0) outer radius b_0 is considered and discretized in N annuli, each having another thickness, which is not selected *a priori*, but is determined during the analysis from the equilibrium equation, given the corresponding stresses, as will be shown later. For mathematical convenience, the radii will be normalized as follows:

$$R_i = r_i / b_0 \,, \tag{17}$$

where r_i denotes the outer radius of the i-th annulus (the first annulus being the outermost one).

Considering that the radial stress σ_r decreases monotonically from the outer boundary (where $\sigma_r = \sigma_0$ and $R_1 = 1$) to the tunnel wall (where $\sigma_r = \sigma_a$ and $R_{N+1} = a_0/b_0$), the thicknesses of the annuli are determined such that the radial stress experiences the same reduction $\Delta\sigma_r$

within every annulus. Consequently, the radial stress at the *i*-th radius is lower than the radial stress at the (*i*–1)th radius by $\Delta\sigma_r = (\sigma_a - \sigma_0)/N$.

The analysis starts from the outermost radius ($R_1 = 1$) and continues inwards in a straightforward way. The stresses at the outer boundary are set equal to the initial stress σ_0, the strains are set equal to zero and the value of the hardening parameter is taken equal to a very small value (a value less than 10^{-6} proved to be sufficiently small) in order to trigger the initiation of the algorithm (step 1 in Table 4, which shows the entire sequence of calculations). Then, for the given stresses and strains at the outer (first) radius and assuming that the hardening parameter at the next (second) radius equals the hardening parameter at the outer (first) radius, the radial stress at the next (second) radius is calculated according to Eq. (21) (step 2) as well as the tangential stress, the position, the elastic strains and the plastic strains (6 unknowns in total) using the yield condition (step 3), the equilibrium condition (step 4), the Hooke's equations (step 5) and the strain compatibility and flow rule (step 6), respectively (6 equations in total). This explicit procedure has to be repeated *N* times. The tunnel wall displacement equals the radial displacement of the (*N*+1)th radius, while the outer radius b_0 equals a_0/R_{N+1}. As the SHS model predicts plastic strains right from the start of shearing, the size of the plastic zone around the tunnel is infinite. For this reason, the radius b_0 is always very large compared with the tunnel radius, provided that a very small value is assigned to the shear strain at the outer boundary.

Validation of the computational method

The computational method is validated with an analytical solution that can be derived under the following conditions: (a), the unloading-reloading modulus is very large compared to the E_{50} secant modulus (*i.e.* the elastic strains are negligible); (b), the mobilized dilation angle is constant (*i.e.* the plastic flow rule is given by Eq. 5); and, (c), the exponent *n* in the power law

Accepted manuscript doi:
10.1680/jgeot.17.p.008

(Eq. 3) equals unity. The first two assumptions fix the strain and displacement distributions around the opening. Specifically, integrating the flow rule over the entire deformation history of a material point ($\varepsilon_r = -\kappa\varepsilon_t$), considering the kinematic relations ($\varepsilon_r = \mathrm{d}u/\mathrm{d}r$ and $\varepsilon_t = u/r$, with inward displacements defined as positive) and finally integrating the resulting differential equation over [a_0, r], given the displacement at the tunnel wall, results in

$$\gamma^{pl} \cong \gamma = (\kappa+1)\varepsilon_t = \frac{u_a}{a_0}\frac{\kappa+1}{(r/a_0)^{\kappa+1}}. \tag{18}$$

Substituting Eq. (18) and the yield condition (Eq. 10 without the elastic term) into the equilibrium equation, and integrating the derived equation over [a_0, b_0], leads to the following closed-form solution for the support pressure:

$$\bar{\sigma}_a = \bar{\sigma}_0 \left[\frac{C_1/C_2 + \gamma_b}{C_1/C_2 + (\kappa+1)u_a/a_0}\right]^{\frac{1}{(\kappa+1)C_2}}, \tag{19}$$

where the constants

$$C_1 = \frac{3}{4}\frac{\bar{\sigma}_{3,ref}}{E_{50,ref}}, \quad C_2 = R_f\left(\frac{2\sin\varphi_f}{1-\sin\varphi_f}\right)^{-1}. \tag{20}$$

The radius b_0 can be determined by means of Eq. (18) setting the deviatoric strain equal to γ_b (γ_b should be taken equal to a very small value as in the previous section; here, it was taken equal to 10^{-6}), while the corresponding stress boundary condition is defined by the initial isotropic stress σ_0. Eq. (19) is valid as long as failure conditions are not satisfied (*i.e.* $q < q_f$) and therefore may apply up to a certain support pressure upon unloading. It applies over the entire range of support pressures only in the special case that the constant R_f equals unity. Figure 16 plots the ground response curve (GRC) according to Eq. (19) (dashed curve) and the curve obtained from the computational method of Table 4 with $E_{ur} = 100E_{50}$, $n = 1$, $R_f = 1$ and $\kappa_m = \kappa$ in step 6 (circular marks), for the parameter set of Figure 1 and considering an

800-meter deep tunnel cross section. The computational method was shown to provide highly accurate results that are in perfect agreement with the analytical solution, provided that the number of annuli N is sufficient (specifically, 2000 annuli are considered here and in the rest of the paper). It should be noted that the computational method is generally applicable and was also validated for other constitutive models for which closed-form solutions for the GRC exist, such as the MC model.

Figure 16 shows that small strain theory may predict for a high deformability and low strength material very large displacements in many cases (even greater than the tunnel radius). However, small strain theory is sufficiently accurate up to convergences of 10%. Therefore, large strain effects will be considered in the following sections using the relationship of Vrakas & Anagnostou (2015), according to which small strain convergences are corrected by means of a simple hyperbolic function of the small strain convergences themselves (the tunnel convergences then always read from 0 to 100%). Although this relationship was proven to be generally applicable, a validation of the corrected small strain results will be performed here for the sake of completeness.

Specifically, integration of the flow rule considering the logarithmic definition of strains ($\varepsilon_r = \ln\left(1+\mathrm{d}u/\mathrm{d}r\right)$ and $\varepsilon_t = \ln\left(1+u/r\right)$) results in

$$\gamma^{pl} \cong \gamma = \left(\kappa+1\right)\varepsilon_t = \ln\left(1+\frac{A}{\left(r/a\right)^{\kappa+1}}\right), \tag{21}$$

where r denotes the current position of a material point, a is the current tunnel radius (in the deformed configuration), and A is a function of the given tunnel convergence:

$$A = \left(1-\frac{u_a}{a_0}\right)^{-(\kappa+1)} - 1. \tag{22}$$

Accepted manuscript doi:
10.1680/jgeot.17.p.008

Integrating then the equilibrium equation (with the aid of Eqs. 10 and 21) over [a, b], where b denotes the current outer radius, leads to the following solution for the support pressure:

$$\bar{\sigma}_a = \bar{\sigma}_0 \exp\left[\int_{C_3}^{1} \frac{\ln\left(1+A/x^{\kappa+1}\right)}{C_1 + C_2 \ln\left(1+A/x^{\kappa+1}\right)} \frac{\mathrm{d}x}{x}\right], \tag{23}$$

where the integration constant C_3 represents the ratio b/a and is obtained from Eq. (21) setting the boundary shear strain equal to γ_b:

$$C_3 = \left(\frac{A}{\exp\left(\gamma_b\right)-1}\right)^{\frac{1}{\kappa+1}}. \tag{24}$$

Figure 16 includes the large strain GRC according to Eq. (23) (solid curve) and the corresponding corrected small strain curve with the relationship of Vrakas & Anagnostou (2015) (triangular marks). The results are in perfect agreement.

Accepted manuscript doi:
10.1680/jgeot.17.p.008

NOTATION

A	function of the tunnel convergence
a, a_0	current and initial tunnel radius
b, b_0	current and initial outer radius
C_1, C_2, C_3	constants
c_f	cohesion at failure
E, E_{ref}	Young's modulus, reference value
E_{50}, $E_{50,ref}$	secant modulus in primary loading at half the q_f, reference value
E_{MC}	operational elastic modulus for the MC model
E_{ur}, $E_{ur,ref}$	unloading-reloading modulus, reference value
i	index of the i-th radius
N	number of annuli
n	exponent of the power law for the stiffness moduli
q, q_a, q_f	deviatoric stress, asymptotic deviatoric stress, failure deviatoric stress
R_f	constant for SHS model
r	radial distance from tunnel centre
u_a	radial displacement at tunnel wall
$u_{a,MC}$	u_a according to the MC model
$u_{a,SHS}$	u_a according to the SHS model
u_ρ	radial displacement at elasto-plastic boundary
x	auxiliary variable in definite integral
Y	yield function
γ	shear (deviatoric) strain
γ_a, γ_b	shear (deviatoric) strain at $r = a$ and $r = b$
ε_1, ε_3	major and minor principal strain
ε_r, ε_t	radial and tangential strain

ζ	variable indicating type of loading ($\zeta = 1$ plane strain, $\zeta = 2$ triaxial compression)
κ, κ_m	function of the dilation angle at failure, function of the mobilized dilation angle
ν	Poisson's ratio
ρ	radius of plastic zone
σ	normal stress
σ_0	initial isotropic stress
σ_1, σ_3	major and minor principal stress
$\sigma_{3,ref}$	reference value of the minor principal stress
σ_a	support pressure
σ_D	uniaxial compressive strength
σ_r, σ_t	radial and tangential stress
σ_ρ	radial stress at elasto-plastic boundary
φ_c, φ_f, φ_m	critical friction angle, friction angle at failure, mobilized friction angle
ψ_f, ψ_m	dilation angle at failure, mobilized dilation angle

Subscripts

i	i-th radius value

Superscripts

el	elastic strain component
pl	plastic strain component

Accepted manuscript doi:
10.1680/jgeot.17.p.008

REFERENCES

Anagnostou, G. & Kovári, K. (1993). Significant parameters in elastoplastic analysis of underground openings. *Journal of Geotechnical Engineering* **119**, No. 3, 401–419.

Anagnostou, G. & Pimentel, E. (2004). *AlpTransit Gotthard Ceneri Basistunnel, Zwischenangriff Sigirino, Felsmechanische Laborversuche, Schlussbericht (Proben Cen01 bis Cen07)*, Bericht Nr. 040202. Zurich, Switzerland: IGT, ETH Zurich (in German).

Anagnostou, G. & Pimentel, E. (2005). *A9 – Umfahrung Visp, Felsmechanische Laborversuche*, Bericht Nr. 050401. Zurich, Switzerland: IGT, ETH Zurich (in German).

Anagnostou, G., Pimentel, E. & Cantieni, L. (2008). *AlpTransit Gotthard Basistunnel, Teilabschnitt Sedrun, Felsmechanische Laborversuche Los 378, Schlussbericht*, Bericht Nr. 080109. Zurich, Switzerland: IGT, ETH Zurich (in German).

Anagnostou, G., Pimentel, E. & Dong, W. (2010). *Thessaloniki Bypass-Motorway – Seich-Sou Tunnel, Experimental investigations on the strength and deformability of Graphitic Phyllites and Talc Schists*, Report No. 102301. Zurich, Switzerland: IGT, ETH Zurich.

Anagnostou, G., Pimentel, E. & Dong, W. (2011). *Ceneri Base Tunnel – AlpTransit project L841-01, Laboratory triaxial tests on rock material, Report Nr. 1 (Samples SIG_1720, SIG_1603, SIG_1680 and Gbc-SE-1088-R-Nr.1)*, Report No. 112701. Zurich, Switzerland: IGT, ETH Zurich.

Asef, M. R. & Reddish, D. J. (2002). The impact of confining stress on the rock mass deformation modulus. *Géotechnique* **52**, No. 4, 235–241.

Barla, G. (2002). Tunnelling under squeezing rock conditions. In *Advances in Geotechnical Engineering and Tunnelling* (ed D. Kolymbas), pp. 169–268. Berlin: Logos Verlag.

Benz, T., Wehnert, M. & Vermeer, P. A. (2008). A Lode angle dependent formulation of the Hardening Soil model. In *Proceedings of the 12th international conference of IACMAG*, pp. 653–660.

Brown, E. T., Bray, J. W. & Santarelli, F. J. (1989). Influence of stress-dependent elastic moduli on stresses and strains around axisymmetric boreholes. *Rock Mech. Rock Engng* **22**, No. 3, 189–203.

Caquot, A. (1934). *Équilibre des massifs à frottement interne*. Paris: Gauthier-Villars (in French).

Cantieni, L. & Anagnostou, G. (2009). The effect of the stress path on squeezing behavior in tunneling. *Rock Mech. Rock Engng* **42**, No. 2, 289–318.

Duncan, J. M. & Chang, C. Y. (1970). Nonlinear analysis of stress and strain in soils. *Journal of the Soil Mechanics and Foundations Division* **96**, No. 5, 1629–1653.

Duncan Fama, M. E. & Brown, E. T. (1989). Influence of stress dependent elastic moduli on plane strain solutions for boreholes. In *Rock at Great Depth* (eds V. Maury & D. Fourmaintraux), pp. 819–826, Rotterdam: Balkema.

Ewy, R. T. & Cook, N. G. W. (1990). Deformation and fracture around cylindrical openings in rock – I. Observations and analysis of deformations. *Int. J. Rock Mech. Min. Sci. & Geomech. Abstr.* **27**, No. 5, 387–407.

Hoek, E. (2001). Big tunnels in bad rock (The thirty-sixth Karl Terzaghi lecture). J. Geotech. Geoenviron. Eng. **127**, No. 9, 726–740.

Janbu, N. (1963). Soil compressibility as determined by oedometer and triaxial tests. In *Proceedings of the 3rd European Conference on Soil Mechanics and Foundation Engineering*, vol. 1, pp. 19–25.

Janbu, N. (1985). Soil models in offshore engineering. *Géotechnique* **35**, No. 3, 241–281.

Koiter, W. T. (1953). Stress-strain relations, uniqueness and variational theorems for elastic-plastic materials with a singular yield surface. *Quarterly of Applied Mathematics* **11**, No. 3, 350–354.

Kondner, R. L. (1963). Hyperbolic stress-strain response: cohesive soils. *Journal of the Soil Mechanics and Foundations Division* **89**, No. 1, 115–143.

Kovári, K. (1985). The determination of the characteristic line from straight line nomograms. In *Proceedings of the 5th International Conference on Numerical Methods in Geomechanics* (eds T. Kawamoto and Y. Itikawa), pp. 1741–1746. Rotterdam: Balkema.

Kovári, K. (1998). Tunnelling in squeezing rock. *Tunnel* **98**, No. 5, 12–31.

Kovári, K., Amberg, F. & Ehrbar, H. (2000). Mastering of squeezing rock in the Gotthard Base. *World Tunnelling* **13**, No. 5, 234–238.

Kulhawy, F. H. (1975a). Stress deformation properties of rock and rock discontinuities. *Engineering Geology* **9**, No. 4, 327–350.

Kulhawy, F. H. (1975b). Stresses and displacements around openings in homogeneous rock. *Int. J. Rock Mech. Min. Sci. & Geomech. Abstr.* **12**, No. 3, 43–57.

Lade, P. V. & Nelson, R. B. (1987). Modelling the elastic behaviour of granular materials. *Int. J. Numer. Anal. Meth. Geomech.* **11**, No. 5, 521–542.

Lee, Y. K. & Pietruszczak, S. (2008). A new numerical procedure for elasto-plastic analysis of a circular opening excavated in a strain-softening rock mass. *Tunnelling and Underground Space Technology* **23**, No. 5, 588–599.

Lumb, P. (1964). Multi-stage triaxial tests on undisturbed soils. *Civil Engineering and Public Works Review* **59**, 591–595.

Nawrocki, P. A. & Dusseault, M. B. (1995). Modelling of damaged zones around openings using radius-dependent Young's modulus. *Rock Mech. Rock Engng* **28**, No. 4, 227–239.

Panet, M. (1995). *Le calcul des tunnels par la méthode convergence-confinement*. Paris: Presses de l'École Nationale des Ponts et Chaussées (in French).

Pimentel, E. & Anagnostou, G. (2014). *Verzweigungskaverne I – Tunnel Visp, Felsmechanische Laborversuche*, Bericht Nr. 143001. Zurich, Switzerland: IGT, ETH Zurich (in German).

Pimentel, E. & Anagnostou, G. (2017). *Karawanks Tunnel, Triaxial tests – Final Report*, Report No. 164305. Zurich, Switzerland: IGT, ETH Zurich.

Pimentel, E., Dong, W. & Anagnostou, G. (2014). *Semmering Basistunnel, Felsmechanische Laborversuche, Schlussbericht*, Bericht Nr. 143002. Zurich, Switzerland: IGT, ETH Zurich (in German).

Reed, M. B. (1988). The influence of out-of-plane stress on a plane strain problem in rock mechanics. *Int. J. Numer. Anal. Meth. Geomech.* **12**, No. 2, 173–181.

Rowe, P. W. (1962). The stress-dilatancy relation for static equilibrium of an assembly of particles in contact. *Proc. R. Soc. Lond. A* **269**, No. 1339, 500–527.

Saeedy, H. S. & Mollah, M. A. (1988). Application of multistage triaxial test to Kuwaiti soils. In *Advanced triaxial testing of soil and rock, STP29087S* (eds R. Donaghe, R. Chaney and M. Silver), pp. 363–375. West Conshohocken, PA: ASTM International.

Santarelli, F. J., Brown, E. T. & Maury V. (1986). Analysis of borehole stresses using pressure-dependent, linear elasticity. *Int. J. Rock Mech. Min. Sci. & Geomech. Abstr.* **23**, No. 6, 445–449.

Schanz, T., Vermeer, P. A. & Bonnier P. G. (1999). The Hardening Soil model: formulation and verification. In *Beyond 2000 in Computational Geotechnics – 10 Years of PLAXIS International* (ed R. B. J. Brinkgreve), pp. 281–296. Rotterdam: Balkema.

Schanz, T. & Vermeer, P. A. (1996). Angles of friction and dilatancy of sand. *Géotechnique* **46**, No. 1, 145–151.

Schubert, P. & Marinko, T. (1989). Vortrieb des Karawankentunnels im tektonisch stark beanspruchten Südabschnitt. *Felsbau* **7**, No. 2, 65–68.

Verman, M., Singh, B., Viladkar, M. N. & Jethwa, J. L. (1997). Effect of tunnel depth on modulus of deformation of rock mass. *Rock Mech. Rock Engng* **30**, No. 3, 121–127.

Vermeer, P. A. & de Borst, R. (1984). Non-associated plasticity for soils, concrete and rock. *Heron* **29**, No. 3, 1–64.

Vogelhuber, M. (2007). *Der Einfluss des Porenwasserdrucks auf das mechanische Verhalten kakiritisierter Gesteine*. Dissertation Nr. 17079, Institut für Geotechnik, ETH Zürich (in German).

Vrakas, A. & Anagnostou, G. (2014). A finite strain closed-form solution for the elastoplastic ground response curve in tunnelling. *Int. J. Numer. Anal. Meth. Geomech.* **38,** No. 11, 1131–1148.

Vrakas, A. & Anagnostou, G. (2015). A simple equation for obtaining finite strain solutions from small strain analyses of tunnels with very large convergences. *Géotechnique* **65**, No. 11, 936–944.

Zytynski, M., Randolph, M. F., Nova, R. & Wroth, C. P. (1978). On modelling the unloading-reloading behaviour of soils. *Int. J. Numer. Anal. Meth. Geomech.* **2**, No. 1, 87–94.

Accepted manuscript doi:
10.1680/jgeot.17.p.008

Table 1. Material constants from CD-TC tests on kakirites from the Gotthard base tunnel (in the multi-stage tests, ψ_f, σ_3, E_{ur} and E_{50} refer to the first loading stage)

No.	Sample	Load stages	c_f [MPa]	φ_f [deg]	ψ_f [deg]	σ_3 [MPa]	E_{ur} [MPa]	E_{50} [MPa]
First experimental campaign (Vogelhuber, 2007)								
1	2	3	0.394	24.4	–	1.5	600	110
2	14.1	1	0.140	28.8	3.5	1.0	700	170
3	14.2	1	0.140	28.8	3.4	6.0	1910	660
4	16.1	1	0.310	28.4	3.2	8.5	4300	1110
5	16.2	1	0.310	28.4	3.6	3.5	1550	220
6	21	4	1.184	31.7	–	1.5	1240	350
7	33	1	0.280	28.2	6.4	1.0	700	190
8	35	1	0.280	28.2	4.6	6.0	2390	620
9	34	4	0.685	27.0	–	1.5	990	260
10	42	1	1.690	23.2	5.2	3.5	1535	530
11	43	1	1.690	23.2	4.7	8.5	2610	830
12	46	1	0.010	25.3	2.7	1.0	995	110
13	47	1	0.010	25.3	2.9	6.0	2045	450
14	50	4	0.720	20.4	–	1.5	1410	490
15	66	3	0.440	30.2	–	1.5	1400	260
16	4	3	0.762	27.0	–	1.5	480	90
17	5	1	1.200	22.5	4.5	3.5	2160	700
18	6	1	1.200	22.5	4.2	8.5	2830	930
19	8	4	0.374	28.8	–	1.5	1080	220
20	11.1	1	0.530	24.2	3.7	6.0	2740	680
21	11.2	1	0.530	24.2	7.7	1.0	910	190
22	12.1	1	0.400	23.4	5.4	3.5	1140	330
23	12.2	1	0.400	23.4	3.6	8.5	2615	870
24	13	3	0.555	28.3	–	1.5	930	170
25	15.1	1	0.320	23.5	3.0	6.0	1945	310
26	15.2	1	0.320	23.5	5.2	1.0	580	90
27	19	4	0.437	26.6	–	1.5	950	280
28	20.1	1	1.080	27.4	5.5	3.5	2025	590
29	20.2	1	1.080	27.4	3.9	8.5	3740	1350
30	22	4	0.368	22.9	–	1.5	890	260
31	23	3	0.299	22.9	–	1.5	790	190
32	26	1	1.040	20.6	6.7	1.0	1390	370
33	27	1	1.040	20.6	2.7	6.0	2850	590
34	36	4	0.383	24.3	–	1.5	770	180
35	37	4	0.450	26.1	–	1.5	900	240
36	39	1	1.260	22.4	6.0	3.5	1885	470
37	41	1	1.260	22.4	4.1	8.5	3070	760
38	48	1	0.390	19.1	4.9	1.0	710	130
39	49	1	0.390	19.1	2.4	6.0	2460	340
40	74	3	0.453	25.4	–	1.5	970	230
41	81	3	0.251	25.9	–	1.5	1050	150

42	84.1	3	0.517	26.3	–	1.5	860	290
43	85.1	1	0.520	32.1	5.4	3.5	2910	570
44	85.2	1	0.520	32.1	3.6	8.5	5450	1060
45	85.3	4	0.608	31.2	–	1.5	1280	260
46	85.4	4	0.754	31.2	–	1.5	2090	440
47	88.2	3	0.384	30.9	–	1.5	1050	210
48	89.1	1	0.800	29.1	5.0	3.5	1850	360
49	89.2	1	0.800	29.1	4.2	8.5	3005	540
50	90.1	1	0.380	26.9	3.5	6.0	3735	580
51	90.2	1	0.380	26.9	4.7	1.0	1340	140
52	91.1	1	0.120	30.8	5.5	3.5	1910	330
53	91.2	1	0.120	30.8	4.8	8.5	3450	760
54	93.1	1	0.640	33.5	4.3	6.0	3825	1400
55	93.2	1	0.640	33.5	5.7	1.0	1080	290
Second experimental campaign (Anagnostou *et al.*, 2008)								
56	34	3	0.096	29.6	3.4	2.0	1100	150
57	35	3	0.010	31.2	2.5	2.0	900	165
58	36	3	0.256	24.9	8.7	2.0	1000	245
59	37	3	0.337	35.1	10.7	2.0	1450	385
60	38	3	0.202	28.5	5.5	2.0	1600	210
61	42	3	0.231	28.1	4.7	2.0	2600	460
62	43	3	0.173	25.8	7.2	2.0	1800	250
63	44	3	0.167	29.6	8.3	2.0	2250	310
64	45	3	0.191	29.1	4.8	2.0	1700	300
65	46	3	0.283	28.8	6.1	2.0	2000	345
66	47	3	0.633	28.8	6.4	2.0	2400	315
67	48	3	0.972	30.6	9.4	2.0	2250	445
68	49	3	0.385	32.6	4.9	2.0	1800	365
69	50	3	0.592	32.3	10.1	2.0	1800	335
70	59	3	0.433	26.2	7.5	2.0	2250	355
71	61	3	0.385	25.2	4.6	2.0	2100	385
72	66	3	0.015	24.9	7.6	2.0	900	140
73	71	3	0.198	26.1	5.8	2.0	1500	130
74	73	3	0.143	25.1	2.7	2.0	1400	60
75	75	3	0.333	20.8	4.3	2.0	1550	90
76	77	3	0.160	32.0	6.4	2.0	1600	255
77	78	3	0.326	23.8	5.0	2.0	2150	140
78	79	3	0.383	29.1	8.4	2.0	3000	380
79	82	3	0.441	28.7	8.4	2.0	2300	270
80	86	3	0.198	32.2	10.1	2.0	1200	220
81	88	3	0.524	29.1	8.9	2.0	850	185
82	89	3	0.309	25.0	5.6	2.0	1500	220
83	90	3	0.336	26.7	8.8	2.0	1300	200
84	91	3	0.528	28.7	10.2	2.0	1000	235
85	92	3	0.422	29.6	10.1	2.0	1250	225
86	94	3	0.358	27.0	2.8	2.0	650	120

87	95	3	0.541	29.9	6.4	2.0	1150	265
88	96	3	0.420	30.4	6.1	2.0	1250	305
89	97	3	0.569	30.0	6.4	2.0	950	210
90	98	3	0.508	26.8	5.2	2.0	700	200

Table 2. Stress-dependency of the unloading-reloading stiffness modulus (Eq. 3; Fig. 5) for the materials tested (the constant *n* was calculated using the least squares method)

Tunnel	Rock type	Number of samples	Number of E_{ur}–values	Exponent *n*
Gotthard (Switzerland)	Kakirites from the Sedrun section	90 [a]	346	0.78
Ceneri (Switzerland)	Fault material from the geological fault zone 'Linea Val Colla' in the Sigirino section	3 [b]	8	0.70
Visp (Switzerland)	Kakirites	2 [b]	9	1.00
Seich-Sou (Greece)	Graphitic phyllites and talc schists	3 [b]	7	0.84
Semmering (Austria)	Sericite phyllites, tectonic breccias and cataclasites	11 [b]	66	0.70
Karawanks (Slovenia)	Tectonically deformed shales, siltstones and claystones	4 [b]	12	0.60

[a] 36 single-stage and 54 multi-stage drained triaxial compression tests

[b] Multi-stage drained triaxial compression tests

Accepted manuscript doi:
10.1680/jgeot.17.p.008

Table 3. Values considered in the parametric study

Poisson's ratio	v	0.3
Friction angle at failure	φ_f	15°/20°/25°/30°
Dilation angle at failure (Vermeer & de Borst, 1984)	ψ_f	max (0° ; $\varphi_f - 20°$)
In situ stress to UCS	σ_0/σ_D	2.5/5/10
Reference confining stress	$\sigma_{3,ref}$	0
Unloading-reloading modulus to UCS	$E_{ur,ref}/\sigma_D$	500/1000/1500
Secant to unloading-reloading modulus	$E_{50,ref}/E_{ur,ref}$	0.15/0.25/0.35
Exponent of the stiffness power law	n	0.2/0.6/1
Failure ratio (= q_f/q_a)	R_f	0.9
Support pressure to *in situ* stress	σ_a/σ_0	0/0.1/0.2/0.3/0.4

Accepted manuscript doi:
10.1680/jgeot.17.p.008

Table 4. Algorithm for calculating the stresses, strains and displacements around a circular tunnel of radius a_0, support pressure σ_a and far-field stress σ_0, assuming that the ground satisfies the SHS model and is discretized in N annuli

1. Set: $i=1,\quad R_1=1,\quad \sigma_{r,1}=\sigma_{t,1}=\sigma_0,\quad \varepsilon_{r,1}^{el}=\varepsilon_{t,1}^{el}=\varepsilon_{r,1}^{pl}=\varepsilon_{t,1}^{pl}=0,\quad \gamma_1^{pl}=10^{-6}$
2. Calculate: $\Delta\sigma_r=\left(\sigma_a-\sigma_0\right)/N$
3. Set: $i=i+1$
4. Calculate the radial stress: $\sigma_{r,i}=\sigma_{r,i-1}+\Delta\sigma_r$
5. Calculate the deformation moduli: $E_{50,i}=E_{50,ref}\left(\bar{\sigma}_{r,i}/\bar{\sigma}_{3,ref}\right)^n,\quad E_{ur,i}=E_{ur,ref}\left(\bar{\sigma}_{r,i}/\bar{\sigma}_{3,ref}\right)^n$
6. Calculate the failure and asymptotic deviatoric stresses: $q_{f,i}=\dfrac{2\sin\varphi_f}{1-\sin\varphi_f}\bar{\sigma}_{r,i},\quad q_{a,i}=q_{f,i}/R_f$
7. Calculate the deviatoric stress using the yield function and setting the value of the hardening parameter equal to its value at the (i–1)th radius: $\dfrac{3}{4}\dfrac{q_i}{E_{50,i}}\dfrac{1}{1-q_i/q_{a,i}}-\dfrac{3}{2}\dfrac{q_i}{E_{ur,i}}-\gamma_{i-1}^{pl}=0$. This quadratic equation can be solved analytically with respect to q_i.
8. If $q_i>q_{f,i}$, set $q_i=q_{f,i}$
9. Calculate the tangential stress: $\sigma_{t,i}=q_i+\sigma_{r,i}$, and $\Delta\sigma_t=\sigma_{t,i}-\sigma_{t,i-1}$
10. Calculate the i-th radius from the equilibrium equation: $R_i=R_{i-1}/\left(1-\Delta\sigma_r/q_i\right)$, and $\Delta R=R_i-R_{i-1}$
11. Calculate the incremental elastic strains from the plane strain Hooke's equations: $\Delta\varepsilon_r^{el}=\dfrac{1+\nu}{E_{ur,i}}\left[\left(1-\nu\right)\Delta\sigma_r-\nu\Delta\sigma_t\right],\quad \Delta\varepsilon_t^{el}=\dfrac{1+\nu}{E_{ur,i}}\left[\left(1-\nu\right)\Delta\sigma_t-\nu\Delta\sigma_r\right]$
12. Calculate the elastic strains: $\varepsilon_{r,i}^{el}=\varepsilon_{r,i-1}^{el}+\Delta\varepsilon_r^{el},\quad \varepsilon_{t,i}^{el}=\varepsilon_{t,i-1}^{el}+\Delta\varepsilon_t^{el}$
13. Calculate the accumulated elastic shear strain: $\gamma_i^{el}=\varepsilon_{t,i}^{el}-\varepsilon_{r,i}^{el}$
14. Calculate the incremental tangential plastic strain from the compatibility equation: $\Delta\varepsilon_t^{pl}=-\left(\Delta R/R_i\right)\left(\gamma_{i-1}^{pl}+\gamma_i^{el}\right)-\Delta\varepsilon_t^{el}$
15. Calculate the incremental radial plastic strain from the plastic flow rule: $\Delta\varepsilon_r^{pl}=-\kappa_{m,i}\Delta\varepsilon_t^{pl}$, where $\kappa_{m,i}$ is determined after Eqs. (13)–(15) considering that $\sin\varphi_{m,i}=q_i/\left(\bar{\sigma}_{t,i}+\bar{\sigma}_{r,i}\right)$
16. Calculate the plastic strains: $\varepsilon_{r,i}^{pl}=\varepsilon_{r,i-1}^{pl}+\Delta\varepsilon_r^{pl},\quad \varepsilon_{t,i}^{pl}=\varepsilon_{t,i-1}^{pl}+\Delta\varepsilon_t^{pl}$
17. Calculate the accumulated plastic shear strain: $\gamma_i^{pl}=\varepsilon_{t,i}^{pl}-\varepsilon_{r,i}^{pl}$
18. Calculate the total strains: $\varepsilon_{r,i}=\varepsilon_{r,i}^{el}+\varepsilon_{r,i}^{pl},\quad \varepsilon_{t,i}=\varepsilon_{t,i}^{el}+\varepsilon_{t,i}^{pl}$
19. If $i<N+1$, go to 3, else end
20. Calculate the outer radius: $b_0=a_0/R_{N+1}$
21. Calculate the radial displacements: $u_i=\varepsilon_{t,i}\times r_i=\varepsilon_{t,i}\times b_0R_i,\quad i=1\div N+1$
22. Calculate the tunnel convergence: $u_a=u_{N+1}$, and 'self-correct' it using the relationship of Vrakas & Anagnostou (2015) to account for large deformations: $u_a/a_0=1-1/\sqrt{1+2\left(u_a/a_0\right)}$

Accepted manuscript doi:
10.1680/jgeot.17.p.008

Figure 1. (a, c) Deviatoric stress vs. axial strain and (b, d) volumetric strain vs. axial strain at σ_3 = 6 MPa (No. 50 in Table 1; upper diagrams) and σ_3 = 1 MPa (No. 51 in Table 1; lower diagrams): results of a CD-TC test on a kakirite sample from the Gotthard base tunnel; MC model predictions and SHS model predictions

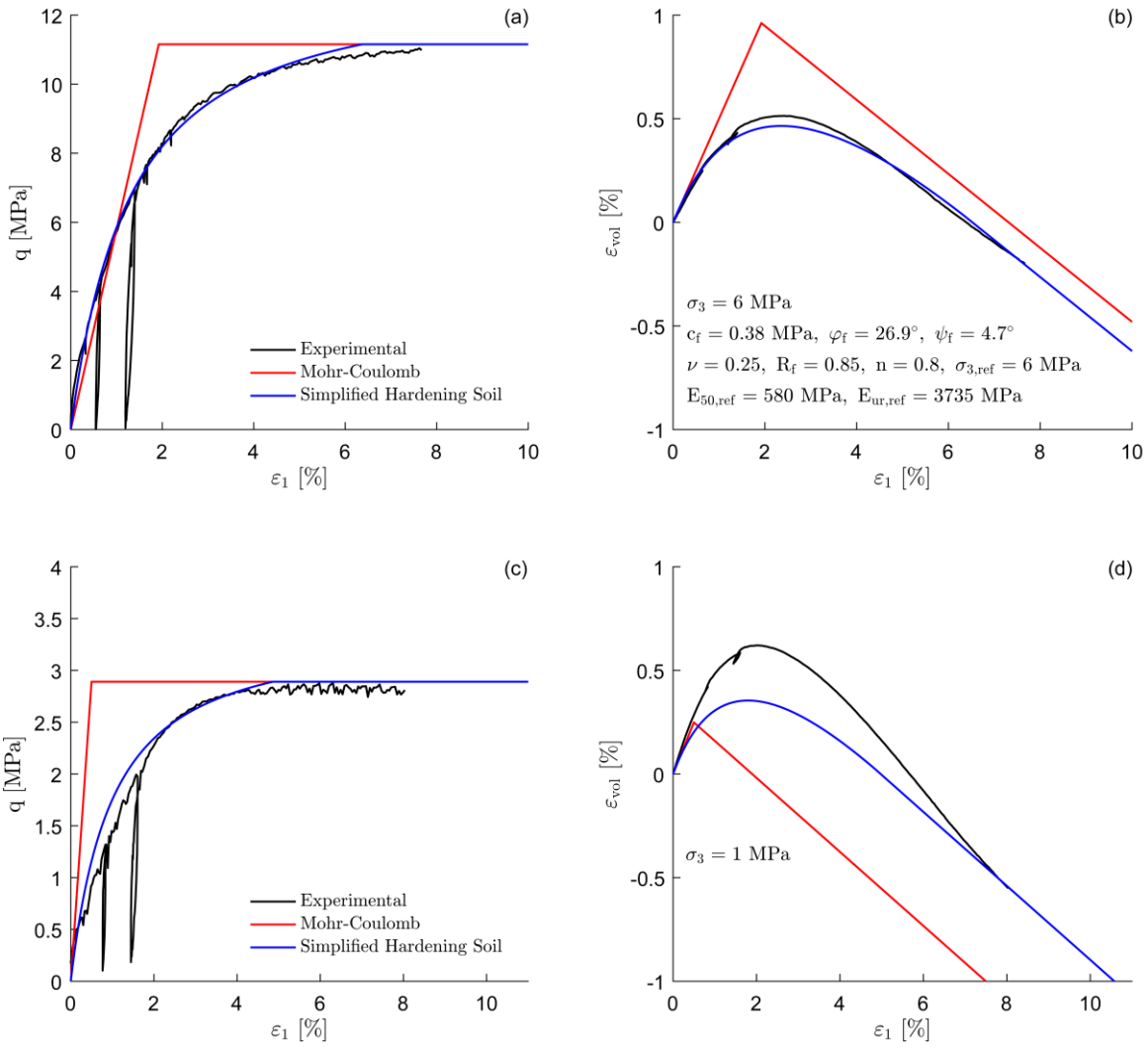

Accepted manuscript doi:
10.1680/jgeot.17.p.008

Figure 2. (a) Deviatoric stress vs. axial strain and (b) volumetric strain vs. axial strain at σ_3 = 2 MPa (No. 63 in Table 1): results of a CD-TC test on a kakirite sample from the Gotthard base tunnel; MC model predictions and SHS model predictions

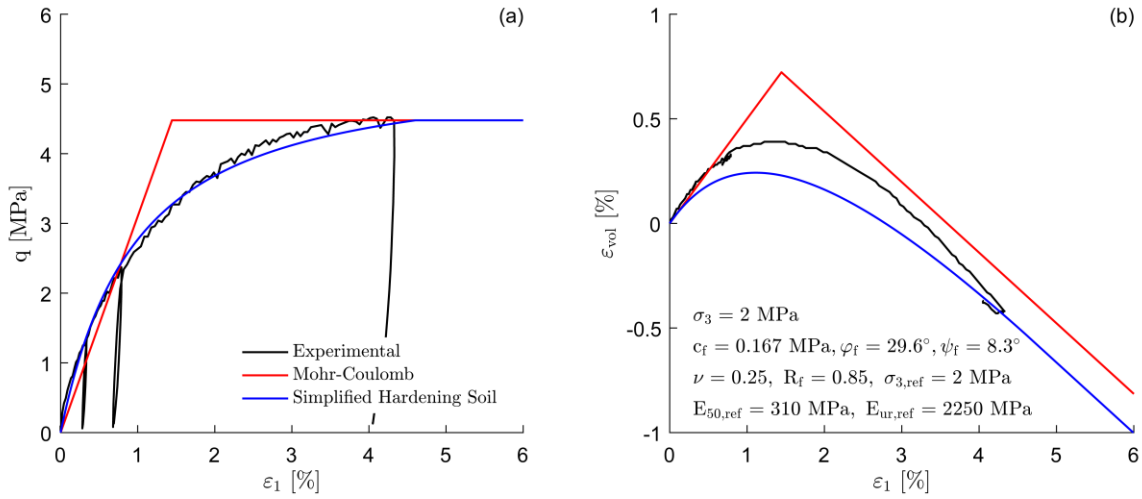

Figure 3. (a) Deviatoric stress vs. axial strain and (b) volumetric strain vs. axial strain at σ_3 = 2 MPa (No. 64 in Table 1): results of a CD-TC test on a kakirite sample from the Gotthard base tunnel; MC model predictions and SHS model predictions

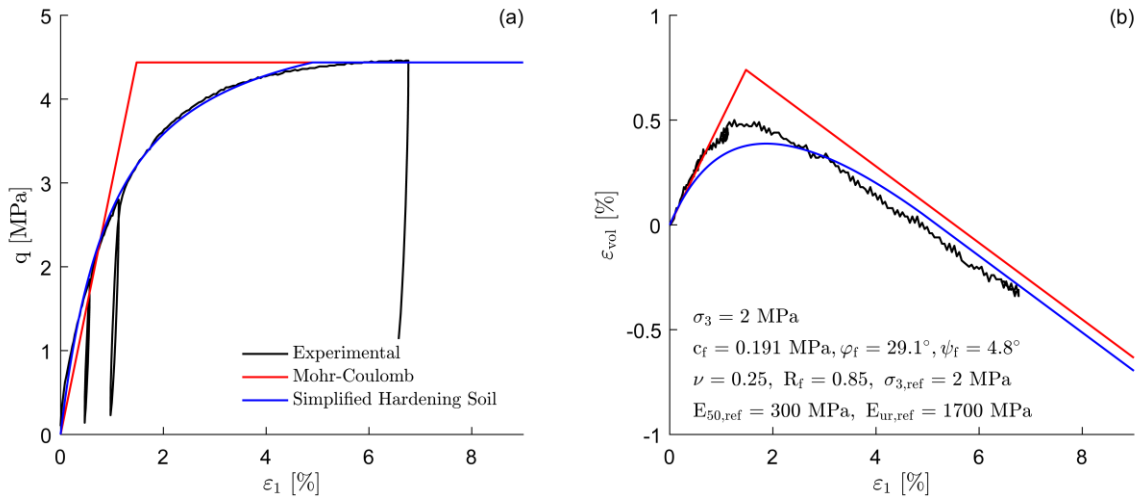

Accepted manuscript doi:
10.1680/jgeot.17.p.008

Figure 4. Schematic representation of the hyperbolic stress-strain relationship in triaxial compression and definition of parameters

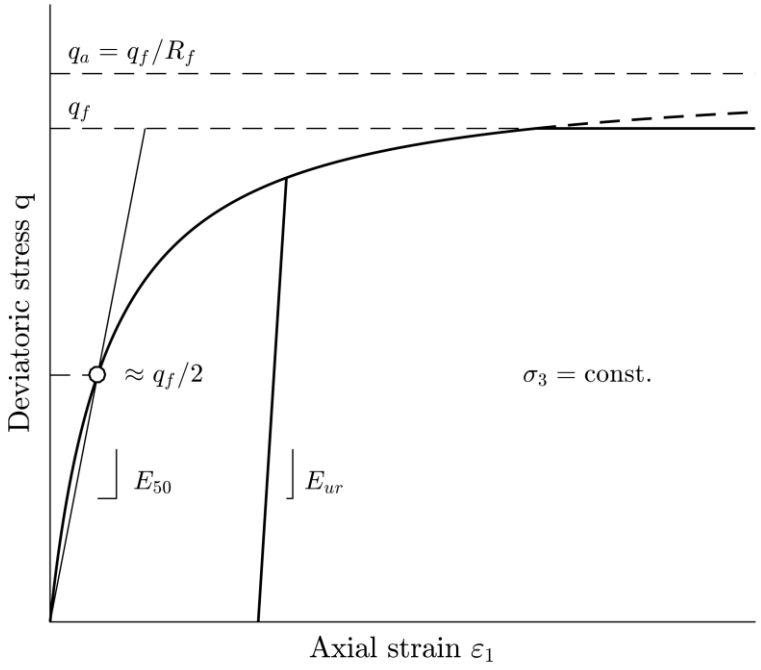

Accepted manuscript doi:
10.1680/jgeot.17.p.008

Figure 5. Stiffness moduli (E_{50} and E_{ur}) of the kakirites from the Sedrun section of the Gotthard base tunnel and of the other materials from the Semmering, Ceneri, Visp, Seich-Sou and Karawanks tunnels over the corresponding transformed confining pressure in bi-logarithmic scale, as determined from triaxial compression tests performed at the Rock Mechanics Laboratory of ETH Zurich

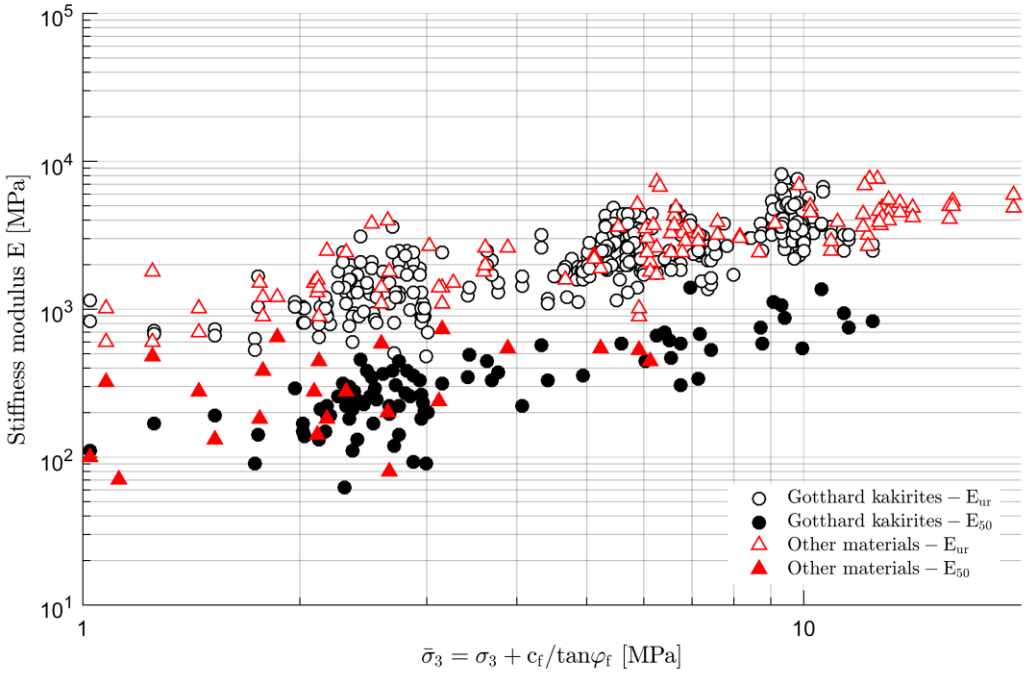

Accepted manuscript doi:
10.1680/jgeot.17.p.008

Figure 6. (a) Deviatoric stress vs. axial strain and (b) volumetric strain vs. axial strain at σ_3 = 1.5 MPa (sample Cen01 in Anagnostou & Pimentel, 2004): results of a CD-TC test on fault material from the Ceneri base tunnel; MC model predictions and SHS model predictions

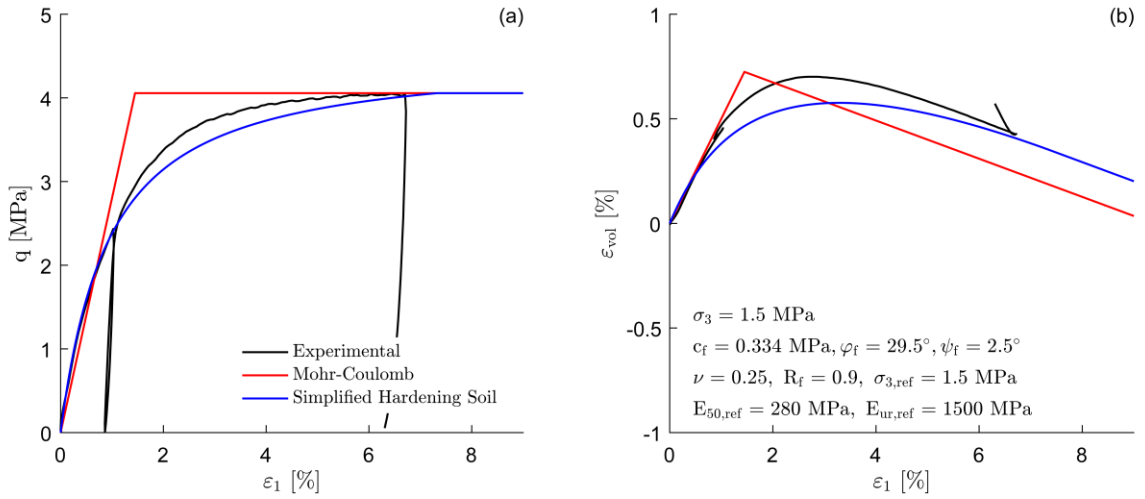

Figure 7. (a) Deviatoric stress vs. axial strain and (b) volumetric strain vs. axial strain at σ_3 = 1.5 MPa (sample Visp02 in Anagnostou & Pimentel, 2005): results of a CD-TC test on kakirite from the Visp tunnel; MC model predictions and SHS model predictions

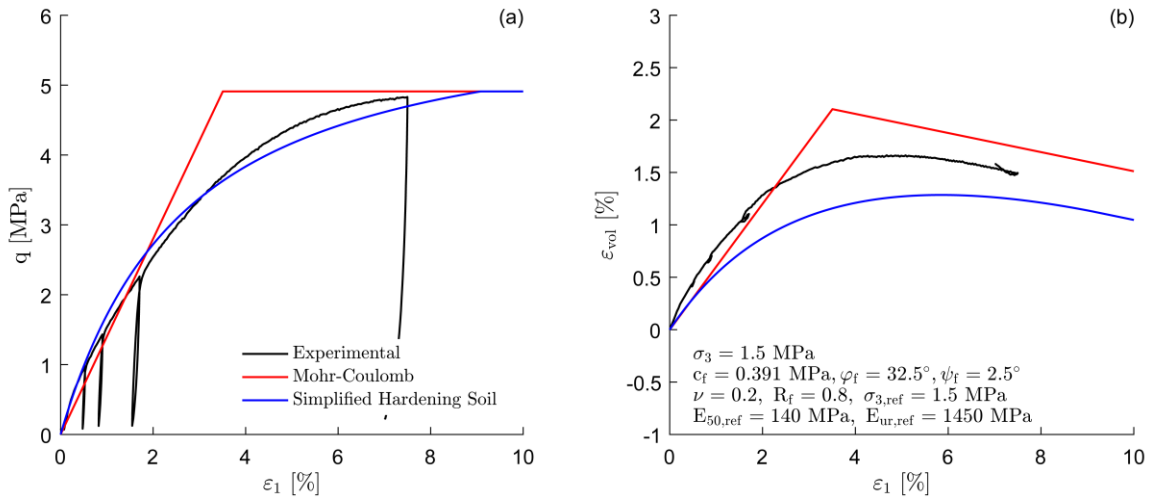

Accepted manuscript doi:
10.1680/jgeot.17.p.008

Figure 8. (a) Deviatoric stress vs. axial strain and (b) volumetric strain vs. axial strain at σ_3 = 1.5 MPa (sample 2150-2170 in Anagnostou *et al.*, 2010): results of a CD-TC test on phyllite from the Seich-Sou tunnel; MC model predictions and SHS model predictions

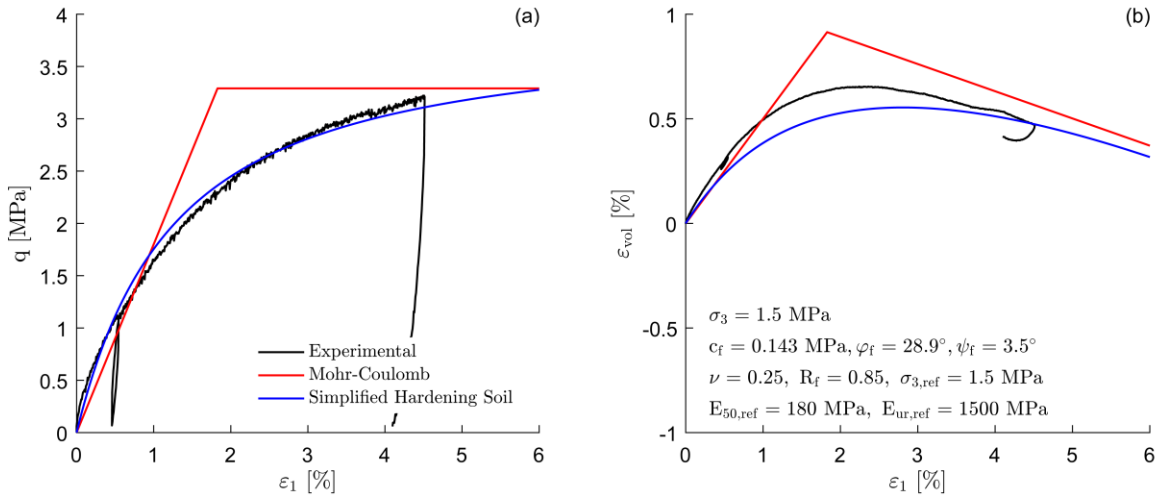

Figure 9. (a) Deviatoric stress vs. axial strain and (b) volumetric strain vs. axial strain at σ_3 = 1 MPa (sample T432.30 in Pimentel *et al.*, 2014): results of a CD-TC test on phyllite from the Semmering base tunnel; MC model predictions and SHS model predictions

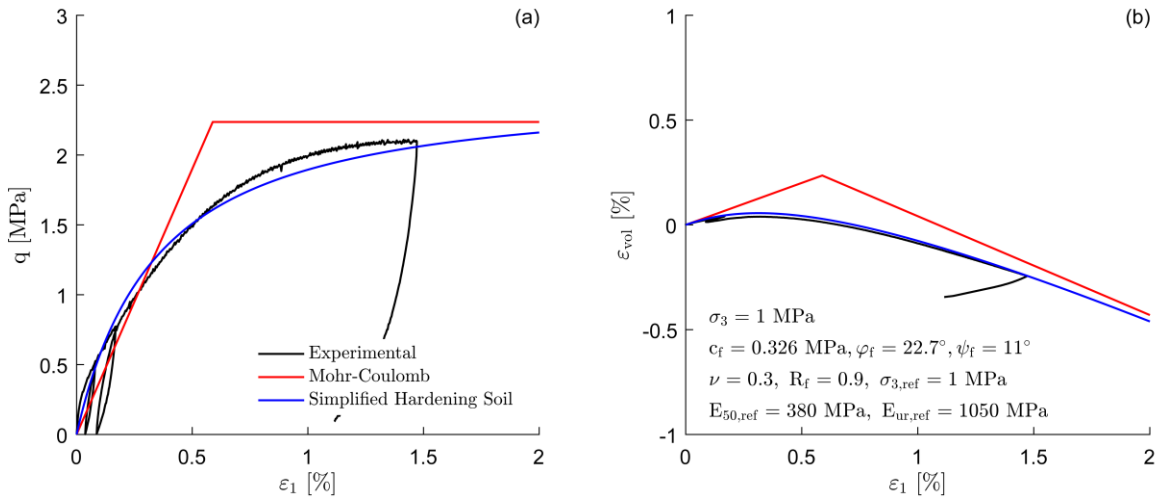

Accepted manuscript doi:
10.1680/jgeot.17.p.008

Figure 10. (a) Deviatoric stress vs. axial strain and (b) volumetric strain vs. axial strain at σ_3 = 2 MPa (sample KG2-T359.6-360.0 in Pimentel & Anagnostou, 2017): results of a CD-TC test on tectonically deformed siltstone from the Karawanks tunnel; MC model predictions and SHS model predictions

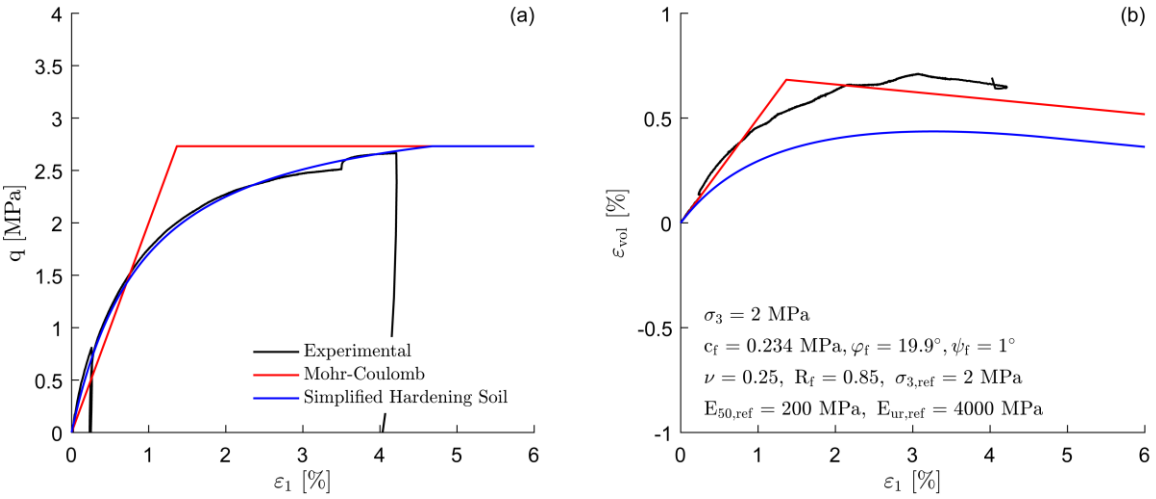

Figure 11. Normalized distributions of (a) the radial and tangential stresses and (b) the shear strain around an axisymmetric tunnel according to the SHS and the MC models (application example for the Gotthard base tunnel)

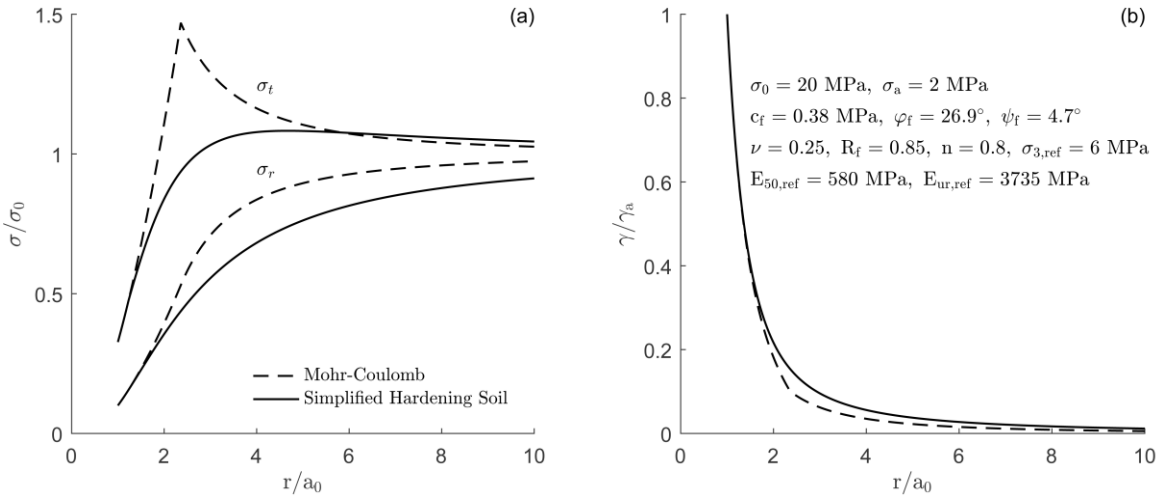

Accepted manuscript doi:
10.1680/jgeot.17.p.008

Figure 12. Ground response curves according to the SHS and the MC models (application example for the Gotthard base tunnel; the elastic moduli considered in the MC model satisfy Eq. 3 with E_{50} or E_{ur} at stress levels of 1, 10 or 20 MPa)

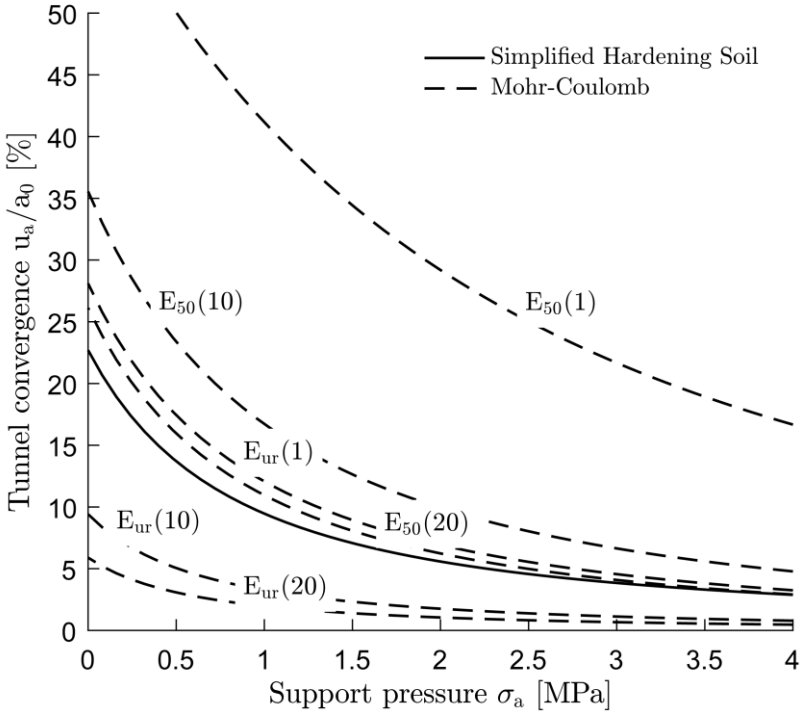

Figure 13. Ground response curves according to the SHS model for (a) fixed E_{50} and varying E_{ur} and (b) fixed E_{ur} and varying E_{50} (application example for the Gotthard base tunnel)

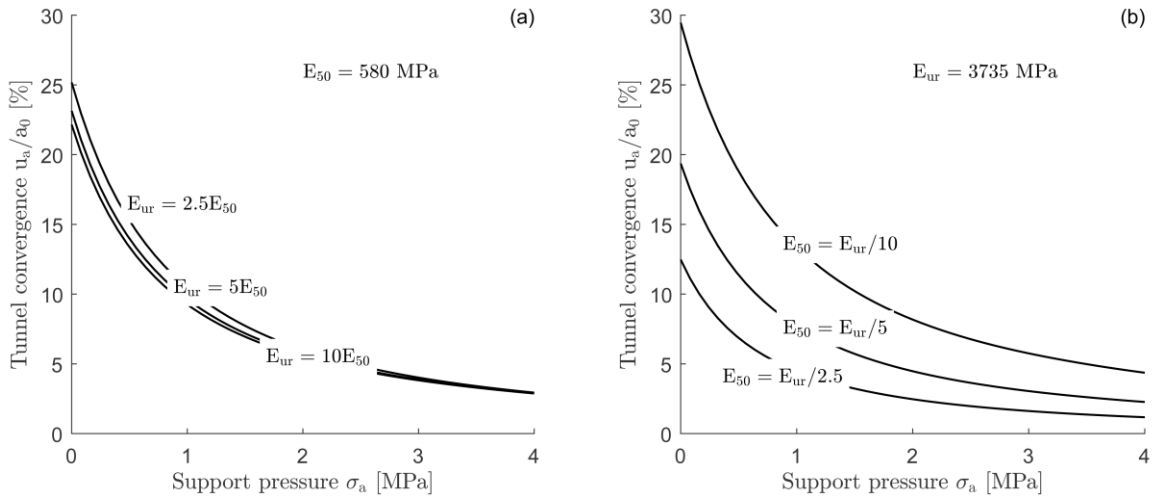

Accepted manuscript doi:
10.1680/jgeot.17.p.008

Figure 14. Relationship between the MC (with an elastic modulus according to Eq. 16) and the SHS unsupported tunnel convergence (90 sets after the experimental results for the Gotthard of Table 1, v = 0.25, n = 0.8, R_f = 0.85; σ_0 = 20 MPa)

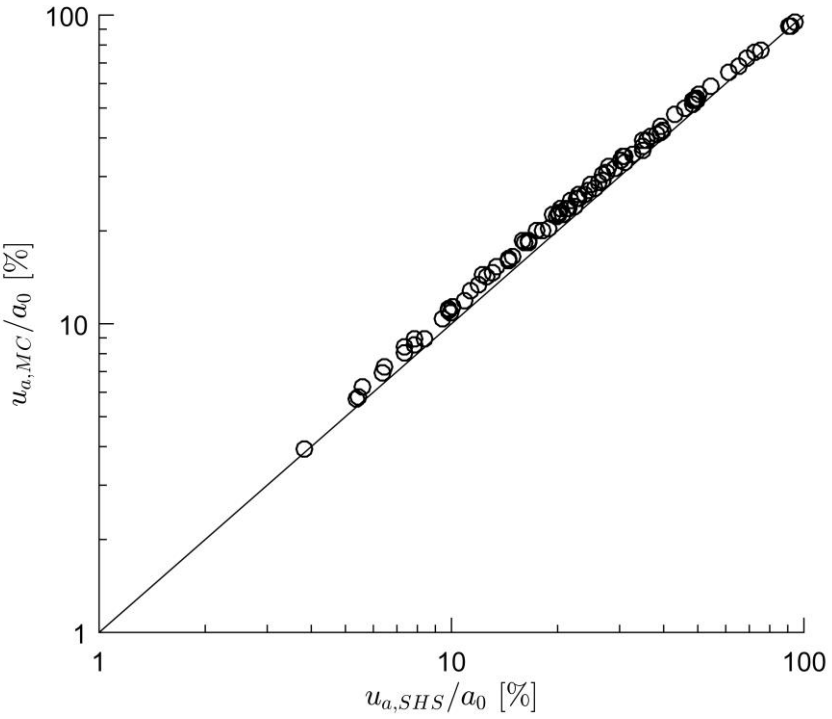

Accepted manuscript doi:
10.1680/jgeot.17.p.008

Figure 15. Relationship between the MC (with an elastic modulus according to Eq. 16) and the SHS tunnel convergence (1620 sets after the parameters of Table 3)

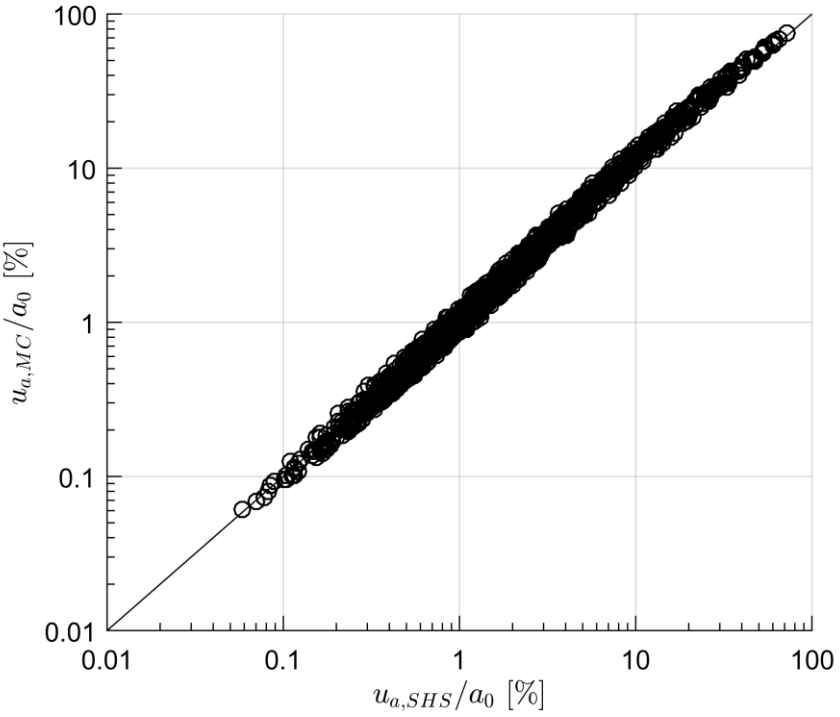

Accepted manuscript doi:
10.1680/jgeot.17.p.008

Figure 16. Ground response curve according to the SHS model for the special case that E_{ur} >> E_{50}, n = 1, R_f = 1 and $\kappa_m = \kappa$ (application example for the Gotthard base tunnel)